



This paper is a part of the hereunder thematic dossier published in OGST Journal, Vol. 70, No. 4, pp. 523-784 and available online [here](#)

Cet article fait partie du dossier thématique ci-dessous publié dans la revue OGST, Vol. 70, n°4, pp. 523-784 et téléchargeable [ici](#)

DOSSIER Edited by/Sous la direction de : **F. Delprat-Jannaud**

Characterization of European CO₂ Storage — European Project SiteChar Caractérisation de sites européens de stockage de CO₂ — Projet européen SiteChar

Oil & Gas Science and Technology – Rev. IFP Energies nouvelles, Vol. 70 (2015), No. 4, pp. 523-784

Copyright © 2015, IFP Energies nouvelles

- 523 > *Editorial – Characterization of European CO₂ Storage – European Project SiteChar*
Éditorial – Caractérisation de sites européens de stockage de CO₂ – Projet européen SiteChar
F. Kalaydjian
- 531 > *SiteChar – Methodology for a Fit-for-Purpose Assessment of CO₂ Storage Sites in Europe*
SiteChar – Une méthodologie pour une caractérisation appropriée des sites de stockage de CO₂
F. Delprat-Jannaud, J. Pearce, M. Akhurst, C.M. Nielsen, F. Neele, A. Lothe, V. Volpi, S. Brunsting and O. Vincké
- 555 > *CO₂ Storage Feasibility: A Workflow for Site Characterisation*
Faisabilité du stockage géologique du CO₂ : une méthodologie pour la caractérisation des sites de stockage
M. Nepveu, F. Neele, F. Delprat-Jannaud, M. Akhurst, O. Vincké, V. Volpi, A. Lothe, S. Brunsting, J. Pearce, A. Battani, A. Baroni, B. Garcia, C. Hofstee and J. Wollenweber
- 567 > *Risk Assessment-Led Characterisation of the SiteChar UK North Sea Site for the Geological Storage of CO₂*
Caractérisation d'un site de stockage géologique de CO₂ situé en Mer du Nord (Royaume-Uni) sur la base d'une analyse de risques
M. Akhurst, S.D. Hannis, M.F. Quinn, J.-Q. Shi, M. Koenen, F. Delprat-Jannaud, J.-C. Lecomte, D. Bossie-Codreanu, S. Nagy, Ł. Klimkowski, D. Gei, M. Plummaekers and D. Long
- 587 > *How to Characterize a Potential Site for CO₂ Storage with Sparse Data Coverage – a Danish Onshore Site Case*
Comment caractériser un site potentiel pour le stockage de CO₂ avec une couverture de données éparées – le cas d'un site côtier danois
C.M. Nielsen, P. Frykman and F. Dalhoff
- 599 > *Coupled Hydro-Mechanical Simulations of CO₂ Storage Supported by Pressure Management Demonstrate Synergy Benefits from Simultaneous Formation Fluid Extraction*
Des simulations du comportement hydromécanique d'un réservoir géologique de stockage de CO₂ dans un contexte de gestion de la pression démontrent les avantages de l'extraction de fluide de la formation au cours de l'injection du CO₂
T. Kempka, C.M. Nielsen, P. Frykman, J.-Q. Shi, G. Bacci and F. Dalhoff
- 615 > *The Importance of Baseline Surveys of Near-Surface Gas Geochemistry for CCS Monitoring, as Shown from Onshore Case Studies in Northern and Southern Europe*
Importance des lignes de base pour le suivi géochimique des gaz près de la surface pour le stockage géologique du CO₂, illustration sur des pilotes situés à terre en Europe du Nord et du Sud
S.E. Beaubien, L. Ruggiero, A. Annunziatellis, S. Bigi, G. Ciotoli, P. Deiana, S. Graziani, S. Lombardi and M.C. Tartarello
- 635 > *Structural and Parametric Models of the Załęcze and Żuchłów Gas Field Region, Fore-Sudetic Monocline, Poland – An Example of a General Static Modeling Workflow in Mature Petroleum Areas for CCS, EGR or EOR Purposes*
Modèles structurels et paramétriques de la région des gisements de gaz de Załęcze et Żuchłów, Région monoclinale des Sudètes, Pologne – un exemple du déroulement d'une modélisation statique générale dans des zones de pétrole matures dans un but de CCS, EGR ou d'EOR
B. Papiernik, B. Doligez and Ł. Klimkowski
- 655 > *Numerical Simulations of Enhanced Gas Recovery at the Załęcze Gas Field in Poland Confirm High CO₂ Storage Capacity and Mechanical Integrity*
Des simulations numériques de récupération assistée de gaz sur un gisement de gaz de Załęcze en Pologne confirment les capacités de stockage de CO₂ élevées et l'intégrité mécanique dudit gisement
Ł. Klimkowski, S. Nagy, B. Papiernik, B. Orlic and T. Kempka
- 681 > *Pore to Core Scale Simulation of the Mass Transfer with Mineral Reaction in Porous Media*
Modélisation des phénomènes de transferts de masse dans les milieux poreux soumis à une réaction de surface : de l'échelle du pore à l'échelle de la carotte
S. Bekri, S. Renard and F. Delprat-Jannaud
- 695 > *Evaluation and Characterization of a Potential CO₂ Storage Site in the South Adriatic Offshore*
Évaluation et caractérisation d'un site de stockage potentiel de CO₂ au sud de la Mer Adriatique
V. Volpi, E. Forlin, A. Baroni, A. Estublier, F. Donda, D. Civile, M. Caffau, S. Kuczynsky, O. Vincké and F. Delprat-Jannaud
- 713 > *Southern Adriatic Sea as a Potential Area for CO₂ Geological Storage*
Le sud de l'Adriatique, un secteur potentiel pour le stockage du CO₂
V. Volpi, F. Forlin, F. Donda, D. Civile, L. Facchin, S. Sauli, B. Merson, K. Sinza-Mendieta and A. Shams
- 729 > *Dynamic Fluid Flow and Geomechanical Coupling to Assess the CO₂ Storage Integrity in Faulted Structures*
Couplage des modélisations hydrodynamique et géomécanique pour évaluer l'intégrité d'un stockage de CO₂ dans des structures faillées
A. Baroni, A. Estublier, O. Vincké, F. Delprat-Jannaud and J.-F. Nauroy
- 753 > *Techno-Economic Assessment of Four CO₂ Storage Sites*
Évaluation technico-économique de quatre sites de stockage de CO₂
J.-F. Gruson, S. Serbutoviez, F. Delprat-Jannaud, M. Akhurst, C. Nielsen, F. Dalhoff, P. Bergmo, C. Bos, V. Volpi and S. Iacobellis
- 767 > *CCS Acceptability: Social Site Characterization and Advancing Awareness at Prospective Storage Sites in Poland and Scotland*
Acceptabilité du CCS : caractérisation sociale du site et sensibilisation du public autour de sites de stockage potentiels en Pologne et en Écosse
S. Brunsting, J. Mastop, M. Kaiser, R. Zimmer, S. Shackley, L. Mabon and R. Howell

Pore to Core Scale Simulation of the Mass Transfer with Mineral Reaction in Porous Media

S. Bekri*, S. Renard and F. Delprat-Jannaud

IFP Energies nouvelles, 1-4 avenue de Bois-Préau, 92852 Rueil-Malmaison Cedex - France
e-mail: samir.bekri@ifpen.fr - stephane.renard@ifpen.fr - florence.delprat-jannaud@ifpen.fr

* Corresponding author

Abstract — *Pore Network Model (PNM) is used to simulate mass transfer with mineral reaction in a single phase flow through porous medium which is here a sandstone sample from the reservoir formation of the Pakoslaw gas field. The void space of the porous medium is represented by an idealized geometry of pore-bodies joined by pore-throats. Parameters defining the pore-bodies and the pore-throats distribution are determined by an optimization process aiming to match the experimental Mercury Intrusion Capillary Pressure (MICP) curve and petrophysical properties of the rock such as intrinsic permeability and formation factor. The generated network is used first to simulate the multiphase flow by solving Kirchhoff's laws. The capillary pressure and relative permeability curves are derived. Then, reactive transport is addressed under asymptotic regime where the solute concentration undergoes an exponential evolution with time. The porosity/permeability relationship and the three phenomenological coefficients of transport, namely the solute velocity, the dispersion and the mean reaction rate are determined as functions of Peclet and Peclet-Damköhler dimensionless numbers. Finally, the role of the dimensionless numbers on the reactive flow properties is highlighted.*

Résumé — **Modélisation des phénomènes de transferts de masse dans les milieux poreux soumis à une réaction de surface : de l'échelle du pore à l'échelle de la carotte** — Le PNM (*Pore Network Model*) est utilisé afin de modéliser les transferts de masse induits par des réactions minérales au cours d'un écoulement monophasique dans milieu poreux, représentant ici un échantillon de grès provenant du champ gazier de Pakoslaw (Pologne). L'espace poral est symbolisé au sein du PNM par une géométrie idéalisée comprenant des corps de pores sphériques joints par des gorges de pores cylindriques. Les paramètres définissant la distribution de ces éléments sont estimés par un processus d'optimisation qui permet de reproduire les données expérimentales d'intrusion capillaire par mercure (MICP, *Mercury Intrusion Capillary Pressure*) ainsi que les propriétés pétrophysiques de la roche telles que la perméabilité et le facteur de formation. Le réseau poreux ainsi généré est utilisé dans un premier temps pour simuler les écoulements multiphasiques par résolution des lois de Kirchhoff. Les courbes de pression capillaire et de perméabilité relative sont alors déduites. Dans un second temps, le transport réactif est intégré avec l'hypothèse d'un régime asymptotique pour lequel les concentrations de solutés présentent une évolution exponentielle avec le temps. La relation porosité/perméabilité et les trois coefficients phénoménologiques de transport (vitesse du soluté, dispersion et vitesse moyenne de réaction) sont calculés en fonction des nombres adimensionnels Peclet et Peclet Damkolher. Enfin, le rôle des nombres adimensionnels sur les propriétés de l'écoulement réactif est souligné.

INTRODUCTION

The geo-sequestration of carbon dioxide is an attractive option to reduce the emission of greenhouse gases. However, acidification of brine in place can occur during CO₂ injection in underground reservoirs (Izgec *et al.*, 2008a, b). This acidification might lead to local mineral reaction which can modify the petrophysical properties of the porous media, particularly the porosity and the permeability. Additionally, it can affect the solute displacement through the macroscopic parameters, namely solute velocity \bar{v}^* , dispersion \bar{D}^* and mean reaction rate $\bar{\gamma}^*$ (Algive *et al.*, 2010; Li *et al.*, 2006; Shapiro and Brenner, 1988; Varloteaux *et al.*, 2013a, b).

Reaction rates estimated from laboratory experiments (batch reactor) cannot be directly applied on large scales (Kim and Lindquist, 2011; Kim *et al.*, 2011; Swoboda-Colberg and Drever, 1993; Wood *et al.*, 2007). Swoboda-Colberg and Drever (1993) noticed a factor of roughly 200 between laboratory reaction rates and field observations on 2 m² plots of soil. They attribute partly this discrepancy to the heterogeneity of the porous media and to its impact on the reactive surface repartition. Shapiro and Brenner (1986, 1988) quantified the influence of mineral reaction on the effective reaction rate, but also on the advective and dispersive reactive transport parameters.

As a consequence, modeling of CO₂ transport during a reservoir storage project calls for an accurate determination of these macroscopic parameters and the so-called constitutive K - ϕ laws. Varloteau *et al.* (2013a) give an overview of the existing approaches to investigate reactive flow through porous media. Generally, they take into account the real pore structure. The pore geometry is discretized by cubic voxels and the finite element or finite volume method is used to integrate local equations over each pore voxel (Adler, 1992; Lemaitre and Adler, 1990). However, all these methods are time consuming so that only very limited pore volumes can be addressed. In order to increase the investigated pore volume with both affordable computational resources and reduced impact on the reliability of the results, the pore network model PNM has been used to determine the macroscopic quantities of the reactive transport on core scale.

PNM uses a simplified micro-structure of the porous medium, which is schematized by pore-bodies connected by pore throats. The approach is versatile, and can account for various phenomena occurring at the pore scale. It was originally developed by Fatt (1956) to calculate multiphase flow properties of porous media. It is now used to account for various phenomena occurring at the pore scale, including mineral reaction and mass transfer. Over the last decades, it has been extensively used to simulate basic phenomena such as capillarity and multiphase flow in porous media (Blunt *et al.*, 1995; van Dijke and Sorbie, 2002; Laroche *et al.*,

1999; Øren, 2003; Payatakes and Dias, 1984). This approach was extended recently by Algive *et al.* (2007, 2010) and Varloteaux *et al.* (2013a, b) to infer pore evolutions and changes of petrophysical properties resulting from deposition and dissolution processes involved in CO₂ storage.

In the present work, PNM is used to simulate mass transfer with mineral reaction in a single phase flow through a network representing a sandstone sample taken from reservoir formation of the Pakoslaw gas field (near Załęcze-Zuchłów field, Poland).

1 MODEL DESCRIPTIONS

1.1 Pore Network Construction and Parameters

PNM is based on a conceptual representation of a porous medium in which flow and transport are determined without describing the exact morphology of the medium (Békri *et al.*, 2002; Laroche and Vizika, 2005; Varloteaux *et al.*, 2013a, b). The void space of the porous medium is simplified as a network of bonds (*i.e.*, pore throats) and nodes (*i.e.*, pore bodies) with an idealized geometry (in practice, a cylindrical channel with a circular, square or triangular cross section). This distinction between pore bodies and pore throats and their simplified geometry make complex problems easier to solve by using analytical solutions.

The network is a three-dimensional either regular or irregular lattice structure (Fig. 1). Irregular lattice pore network representation (Fig. 1b) has been recently developed using the real structure of the porous medium so as to get closer to the real medium geometry (Øren and Bakke, 2002; Press *et al.*, 1992; Sok *et al.*, 2002; Youssef *et al.*, 2007). This method has made tremendous progress with synchrotron computed micro-tomography which generates 3D data sets on the micrometer scale. The principle is to capture the resolved pore space of rocks in order to perform partitioning steps that divide pore space into individual pore volumes separated by throat surfaces. Further details can be found in Youssef *et al.* (2007). The main shortcoming of this representation is the constrain on the sample size which has to be smaller than 1 cm across if a 3 microns resolution is expected. The physical phenomena that occur at pore space below such a resolution cannot be taken into account. An alternative representation is to define the pore space as a regular cubic lattice pore network where the spatial distribution of pores and pore-throats are based on available petrophysical laboratory data (Fig. 1a). This representation is widely used to represent natural porous media such as reservoir rocks (Mohanty and Salter, 1982; Békri *et al.*, 2002; Dias and Payatakes,

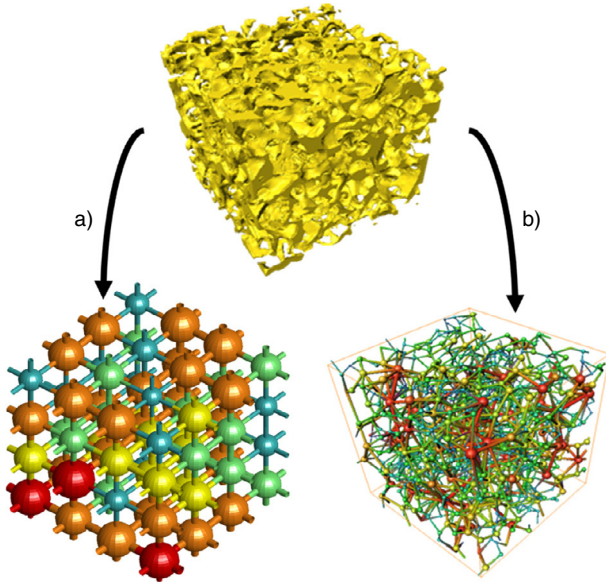


Figure 1

Pore network models: a) model reconstructed with a regular lattice in order to reproduce petrophysical properties of a real porous media (Békri and Vizika, 2006); b) model extracted from the micro tomography images in order to get the same structure as the real rock sample (Youssef et al., 2007).

1986; Fenwick and Blunt, 1998; Heiba et al., 1992; Hoefner and Fohler, 1988; Laroche et al., 1999; McDougall and Sorbie, 1997; Prat, 1995; Stewart and Kim, 2004).

This study is based on the latter representation which consists of a simple lattice network, characterized by a constant co-ordination number. The pore body is assumed to be accessible by six pore throats of identical inscribed diameter (Fig. 1a). The aspect ratio AR between pore-body diameter D and pore-throat diameter d is assumed to be constant. This definition implies that pore-throats, which relate two pore bodies, do not have a constant section; they are defined by two diameters that are randomly generated according to a given probability density function.

The pore body volume is assumed to be proportional to the pore inscribed diameter D to a given exponent, λ_p , following the relationship $V_p(D) \sim D^{\lambda_p}$. This empirical approach has been used by many authors to represent the relationship between radius and volume for real pores (Békri et al., 2002; Heiba et al., 1992; Fenwick and Blunt, 1998). Here the relationship for the pore body volume is $V_p(d) \sim (AR \cdot d)^{\lambda_p}$, since D and d are correlated through the aspect ratio AR . More precisely:

$$V_p(d) = C_p \bar{D}^{(3-\lambda_p)} AR^{\lambda_p} d^{\lambda_p} \quad (1)$$

where C_p is a coefficient that has to be tuned to fit the porosity and \bar{D} the average pore body diameter.

The hydraulic pore throat length l_{ht} is assumed to be correlated to the pore throat radius according to three different scenarios. It can be considered as constant, proportional or inversely proportional to the pore throat radius depending on the value of λ_t :

$$\begin{cases} l_{ht, \lambda_t} = C_t \cdot (L - \bar{D}) \cdot (d/\bar{d})^{\lambda_t} & \text{for } \lambda_t = 0, 1 \\ l_{ht, -1} = C_t \cdot (L - D) & \text{for } \lambda_t = -1 \end{cases} \quad (2)$$

where C_t is a coefficient that has to be tuned to fit the permeability and L the lattice periodicity length (i.e., the node-to-node distance). For a given λ_p and a given pore throat distribution, λ_t , C_p , C_t and L are adjustable parameters that allow to reproduce the rock permeability, porosity and formation resistivity factor obtained through experimental determination.

The determination of an adequate set of values for λ_t , λ_p , C_p , C_t and L including the probability density function $F_n(r)$ of the pore throat diameter is a key step of the construction of a representative pore network based on this cubic structure. These parameters are determined by an optimization process aiming to match the experimental MICP curve and petrophysical properties of the rock (Békri et al., 2002; Békri and Vizika, 2006; Laroche and Vizika, 2005).

1.2 Fluid Flow Modeling

1.2.1 Intrinsic Rock Properties

The intrinsic permeability K of the network is obtained from the Darcy's law at complete saturation. Flow is simulated by applying a macroscopic pressure difference ΔP across the network and assigning a periodic boundary conditions in directions perpendicular to applied ΔP . The local flow rate between pore i and neighbouring pore j is defined by the Poiseuille's law:

$$q_{ij} = \frac{r_t^2 A_t}{8\mu l_{ht}} (P_i - P_j) \quad (3)$$

where subscripts i and j correspond to the i^{th} and j^{th} pore bodies, l_{ht} is the hydraulic length of the ij throat segment, r_t the throat radius, A_t the throat cross section and μ the viscosity of the fluid. In each pore i , mass conservation is imposed. The problem is reduced to a system of linear algebraic equations, the solution of which gives the pressure in the pores. Then the macroscopic flow rate Q is calculated in order to determine the intrinsic permeability.

The analogy to the intrinsic permeability is the formation factor, FF , which defines the conductivity of a porous medium. It is defined as the ratio of the electrical resistivity of the

rock saturated with brine, R_0 , to the resistivity of the brine, R_w :

$$FF = R_0/R_w \quad (4)$$

In order to determine the network resistivity, R_0 , a macroscopic voltage difference ΔU is applied across the network. The induced total current intensity I is then determined by solving for the electrical potential U_i in each node related to the individual electrical current in throats I_{ij} :

$$I_{ij} = \sigma_w \frac{A_{wt}}{l_{hff}} (U_i - U_j) \quad (5)$$

where A_{wt} represents the cross-sectional area occupied by the water phase (bulk or film), l_{hff} is the equivalent electrical length of the throat and σ_w the electrical conductivity of bulk water. Once I is calculated, R_0 can be determined by the Ohm's law.

1.2.2 Two Phase Flow Properties

Using this conceptual schematization of the porous medium, simulations of multiphase flow displacement have been developed, yielding capillary pressure and relative permeability curves. Assuming low capillary numbers, the two phase flow in the network follows a quasi-static displacement. Hence, the capillary pressure curve can be obtained by simulating an invasion-percolation process based on the Young-Laplace equation. An increasing pressure (*i.e.*, P_{NW} , pressure of the non wetting phase) is applied on the injected fluid while the pressure of the fluid in place (*i.e.*, P_w , pressure of the wetting phase) is kept constant. Since the viscous pressure gradients are negligible, the pressure of each phase is assumed to be constant everywhere within the network. All pores connected to an already invaded pore *via* a throat greater than or equal to the equivalent pore entry radius are invaded. The saturation at each capillary pressure (*i.e.*, $P_c = P_{NW} - P_w$) is evaluated from the invaded network elements (*i.e.*, pores and throats). The drainage capillary pressure curve P_c - S is then obtained by stepwisely increasing the capillary pressure and invading the corresponding pores until the entire volume is filled. A detailed description of the calculation can be found in [Laroche and Vizika \(2005\)](#).

The two phase relative permeability curves Kr - S are calculated at each saturation state of the two phase quasi-static displacements once the capillary equilibrium is reached. Similarly to the one phase flow, flow rate of the fluid α (bulk or film) in each segment is given by:

$$q_{ij}^\alpha = g_{h,ij}^\alpha (P_i^\alpha - P_j^\alpha) \quad (6)$$

where P^α stands for the pressure of phase α and $g_{h,ij}^\alpha$ for its conductance. For more information on $g_{h,ij}^\alpha$ the reader can

refer to [Laroche et al. \(1999\)](#). Relative permeabilities can be determined from the macroscopic flow rate Q_α of the phase α by the generalized Darcy's equation.

Similarly to relative permeabilities, determination of electrical resistivity index, $RI = R_t/R_0$, relies on the determination of the electrical resistivity R_t of the partially saturated porous media. In order to obtain R_t the total current intensity is calculated. Local currents are determined from Equation (5) by correctly adapting the cross-sectional area A_{wt} occupied by the water phase.

1.3 Reactive Mass Transport Modeling

An analogous approach to the fluid flow modeling is developed here to address the reactive transport in the case of single phase flow in the limit of long times. Of course, the reactive fluid could be a brine rich in CO_2 . The fluid properties such as pressure, temperature and pH, and mineralogy of the porous media are introduced by the dimensionless numbers Peclet (Pe) and Peclet-Damköhler ($PeDa$):

$$Pe = \frac{\bar{v}\bar{d}}{D_m} \quad \text{and} \quad PeDa = \frac{\kappa\bar{d}}{D_m} \quad (7)$$

where \bar{v} is the mean fluid velocity in the network, \bar{d} the main pore throat diameter, κ the intrinsic reaction rate constant and D_m the molecular diffusion coefficient. Pe compares the diffusion and convection characteristic times and $PeDa$ compares the diffusion and the intrinsic reaction characteristic times.

1.3.1 Concentration Field Computation

A parallel can be drawn between the resolution of the concentration and the pressure field. A comparable reasoning is used to solve the concentration field in the asymptotic regime where the concentration is assumed to decrease exponentially with time ([Shapiro and Brenner, 1986](#)):

$$\frac{\partial \bar{c}}{\partial t} = \lambda_0(\bar{c} - c^*) \quad \text{or equivalently} \quad \bar{c}(z, t) = \bar{c}(z) \exp(-\lambda_0 t) \quad (8)$$

where λ_0 is the equivalent kinetic reaction rate, \bar{c} the mean concentration over the cross section z of the pore network elements (*i.e.*, pore throat or pore body) and c^* the equilibrium concentration.

According to [Algive et al. \(2010\)](#) and [Varloteaux et al. \(2013a, b\)](#), the concentration field along each pore network element can be obtained from an average one dimension formulation of the reactive transport problem:

$$v^* \frac{\partial \bar{c}}{\partial z} - D^* \frac{\partial^2 \bar{c}}{\partial z^2} + (\gamma^* - \lambda_0) (\bar{c} - c^*) = 0 \quad (9)$$

where v^* , D^* and γ^* are pore scale coefficients. [Algive et al. \(2010\)](#) also provide analytical functions which describe the dependencies between these coefficients and the local dimensionless numbers Pe and $PeDa$ defined with the diameter of the considered pore network element.

In the ij pore throat segment modeled by an infinite cylinder of radius R , concentration C_{ij} can be written as function of Bessel functions J_0 and J_1 :

$$c_{ij}(r, z) = \frac{\lambda_0^2}{2PeDa} \frac{J_0\left(\frac{\lambda_0 r}{R}\right)}{J_1(\lambda_0)} \bar{c}_{ij}(z) \quad \text{with} \quad \lambda_0 \frac{J_1(\lambda_0)}{J_0(\lambda_0)} = PeDa \quad (10)$$

In the pore body, concentration C_i is limited to only two forms based either on dominant diffusion or perfect mixing. Perfect mixing results in a uniform concentration $C_i = \bar{c}_i$. In case of dominant diffusion, C_i is controlled by diffusion and mineral reaction in a sphere of radius R :

$$c_i(r) = \frac{\lambda_0^2}{3PeDa} \frac{R \sin\left(\frac{\lambda_0 r}{R}\right)}{r \sin(\lambda_0)} \bar{c}_i \quad \text{with} \quad 1 - \frac{\lambda_0}{\tan \lambda_0} = PeDa \quad (11)$$

Then, the mass balance in each pore body i of the network yields:

$$(\gamma^* - \bar{\gamma}^*) \frac{R^2}{D^*} = \sum_{j=1}^{n_i} \phi_{ij} \quad (12)$$

where ϕ_{ij} are the solute fluxes at the interface between the n_i connected neighbour pore throats (n_i is equal to the coordination number) and the i^{th} pore body. The left side of mass balance equation is the sink-source term of the reaction in the pore body. ϕ_{ij} are derived from the analytical solution of the averaged one dimension equation of the reactive transport. Details of the calculations can be found in [Varloteaux et al. \(2013b\)](#).

1.3.2 Determination of Macroscopic Parameters

The problem is reduced to a system of non linear algebraic equations, the solution of which gives \bar{c} in the pores. Then the macroscopic coefficients $\bar{\gamma}^*$, \bar{v}^* and \bar{D}^* can be calculated thanks to the moment theory adapted to the PNM specifics ([Algive et al., 2010](#); [Varloteaux et al., 2013a, b](#)). They are expressed as functions of the three first spatial moments \mathbf{m}_i of the concentration:

$$\bar{\gamma}^* = -\frac{1}{m_0} \frac{dm_0}{dt}, \quad \bar{v}^* = \frac{d}{dt} \left(\frac{\mathbf{m}_1}{m_0} \right), \quad \bar{D}^* = \frac{d}{dt} \left(\frac{\mathbf{m}_2}{m_0} - \left(\frac{\mathbf{m}_1}{m_0} \right)^2 \right) \quad (13)$$

with

$$\mathbf{m}_i(t) = \int c(\mathbf{r}, t) \mathbf{r}^i d\mathbf{r} \quad (14)$$

Finally, the mineral reaction at the solid liquid interface of the pore network is described by a first order kinetic reaction model. The pore growth/reduction can be expressed as:

$$\frac{\partial R}{\partial t} = -\frac{V_{mS} v_S}{v_F} \kappa [c(r) - c^*] \quad \text{on the interface solid liquid} \quad (15)$$

where V_{mS} is the molar volume of the mineral species; v_S and v_F are the stoichiometric numbers of the mineral and aqueous species related to the mineral reaction, respectively.

The evolution of the pore network geometry due to reaction is computed through an iterative process based on porosity modifications as detailed in [Figure 2](#):

– step 1. For a given initial pore network, the flow field is determined for an arbitrary pressure difference between inlet and outlet. Then, the porosity and the permeability

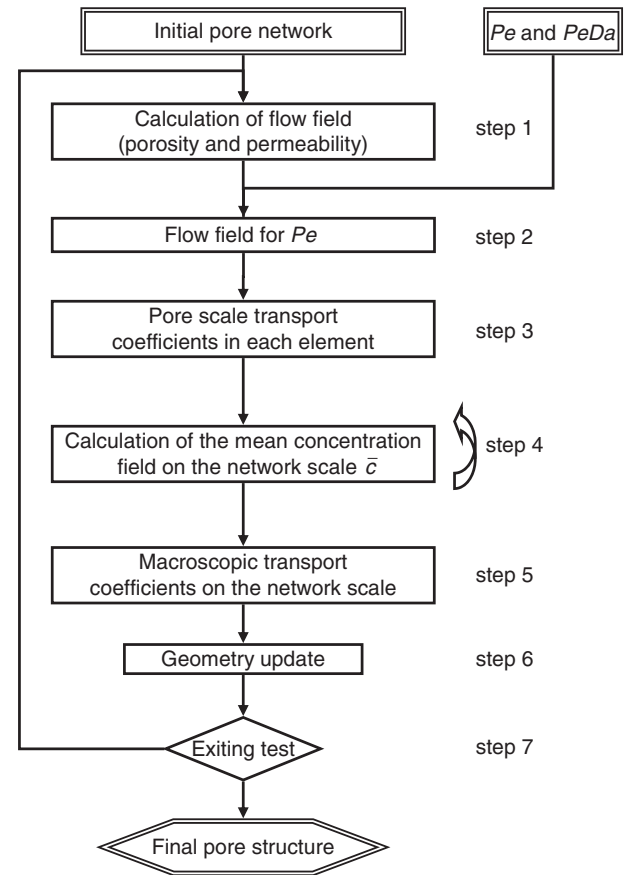


Figure 2

General diagram of the reactive transport solved using PNM.

- of the network are calculated as well as the mean interstitial velocity;
- step 2. The pressure difference, which is directly related to the average velocity through Darcy equation, is adjusted to match the imposed Pe ;
 - step 3. From the analytical formulation provided by [Algive et al. \(2010\)](#), the pore scale transport coefficients v^* , D^* and γ^* are settled for each element of the network;
 - step 4. The concentration field is solved using the iterative Newton-Raphson method ([Press et al., 1992](#));
 - step 5. The macroscopic coefficients $\bar{\gamma}^*$, \bar{v}^* and \bar{D}^* are determined in the direction of applied ΔP ;
 - step 6. The evolution of the geometry is taken into account and a new pore network is obtained;
 - step 7. Step 1 to 6 are iterated to derive the so-called constitutive K - ϕ laws.

2 APPLICATION

2.1 Sample Characteristics

The methodology is applied on a sandstone sample taken from reservoir formation of the Pakoslaw gas field (near Załęcze-Żuchłów site, Poland). It is composed predominantly of quartz, and minor amounts of dolomite, kaolinite and hematite. The petrophysical properties (permeability K , porosity ϕ and formation factor FF) derived from experiments are summarized in [Table 1](#).

Different scenarios described in [Table 2](#) have been tested for various values of exponents λ_p and λ_t to construct a representative pore network of the investigated rock. For each value of exponents λ_p and λ_t the Pore-Throat Size Distribution PSD has been optimized so as to match the experimental MICP curves. The resulting PSD are displayed in terms of

frequency $F_n(r)$ in [Figure 3](#). The prefactors C_p and C_t are tuned to fit the target porosity and permeability. The Formation factor is calculated directly without any matching of experimental data. [Figures 3a](#) and [3b](#) compare the PSD of each scenario to the one obtained from the conventional interpretation of the MICP curve. Differences can be explained by the fact that the conventional interpretation of the MICP curve is based on the hypothesis that the porous medium is a bundle of parallel and non communicating capillary tubes. Injecting this PSD in a network model that takes into account features, such as interconnectivity, aspect ratio, etc., that do not exist in the bundle of capillaries model leads to misfit with the experimental results. This conventional PSD can thus be used only as a first guess and has to be adjusted until the experimental Pc - S curve is fitted, as shown in [Figure 3b](#).

Scenario Run #1 that considers constant pore volume and constant hydraulic length ($\lambda_p = 0$ and $\lambda_t = 0$) leads to a very good agreement between the experimental and simulated Pc curves. It also gives the best prediction in terms of petrophysical parameters such as porosity, permeability and formation factor. The pore networks constructed with the other scenarios do not match the experimental formation factor ([Tab. 1](#)).

The pore network which corresponds to scenario Run #1 will thus be used to calculate the two phase properties and the macroscopic parameter of the reactive flow.

2.2 Two Phase Flow Calculations

The gas/water capillary pressure, relative permeability and resistivity index curves are calculated for a network constructed using the pore-throat size distribution obtained with Run #1 scenario described in [Table 2](#). These data are obtained by simulating a gas invasion in a network initially fully saturated with water (primary drainage process). The results are presented in [Figure 4](#) both in logarithmic and linear coordinates. The relative permeability curves approximately follow the well-known Corey correlation ([Corey, 1954](#)) with an exponent equal to 2 and 5.5 for gas and water, respectively. The saturation exponents obtained in the simulation of the resistivity index is equal to 1.75. It is comparable to the commonly measured exponent in sandstones, which are in the range of 1.7-2.2.

TABLE 1
Petrophysical properties of the selected sample “PaK6-S12p”

Permeability (mDarcy)	Porosity (%)	Formation factor
7.9	18.9	42

TABLE 2
Different scenarios tested to describe the considered reservoir sandstone rock

Run scenarios	Run #1 $\lambda_p = 0; \lambda_t = 0$	Run #2 $\lambda_p = 0.5; \lambda_t = 0$	Run #3 $\lambda_p = 0; \lambda_t = 1$	Run #4 $\lambda_p = 0; \lambda_t = -1$
FF	43.2	112.6	44.3	7.4

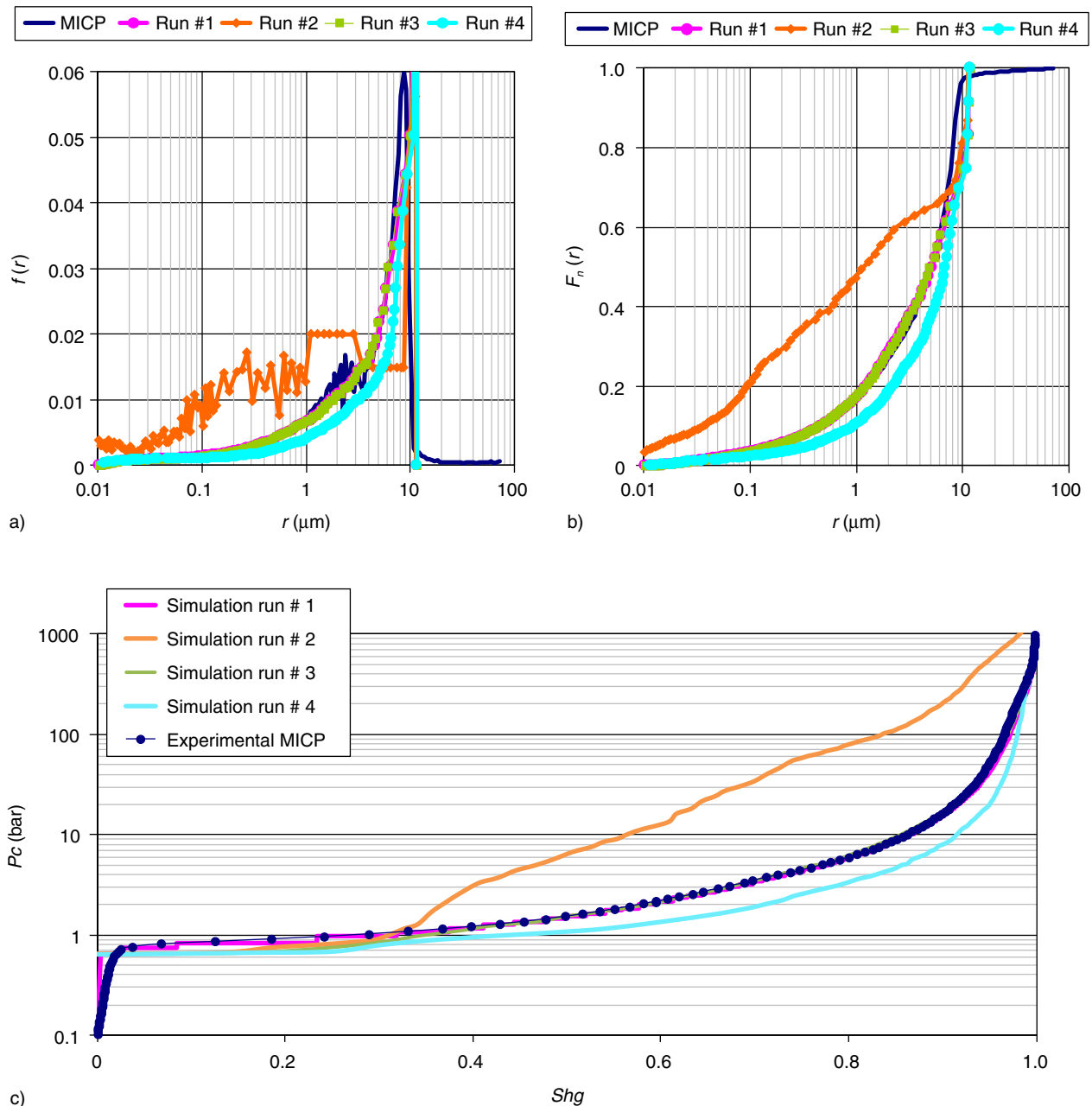


Figure 3

Pore-throat radius distributions, in term of density $f(r)$ a) and cumulative frequency $F_n(r)$ b), obtained with different λ_p and λ_t scenarios (Tab. 2); c) comparison of capillary pressure curves obtained experimentally and by simulations with different pore space geometry scenarios.

These multiphase flow properties calculated on the core scale can be used as input data on the reservoir scale.

2.3 Reactive Flow Simulation

This study focuses on the pore structure of the reservoir sandstone sample. The mineralogy of the grains is

introduced as input data by fixing the intrinsic reaction rate constant κ (i.e., $PeDa$). For simplicity, the chemical interaction at the fluid-rock interface is modeled by a constant κ but heterogeneous distribution of κ could also be taken into account provided data are available to infer the heterogeneity. The reactive transport properties are calculated at core scale for single-phase flow in the limit of long times.

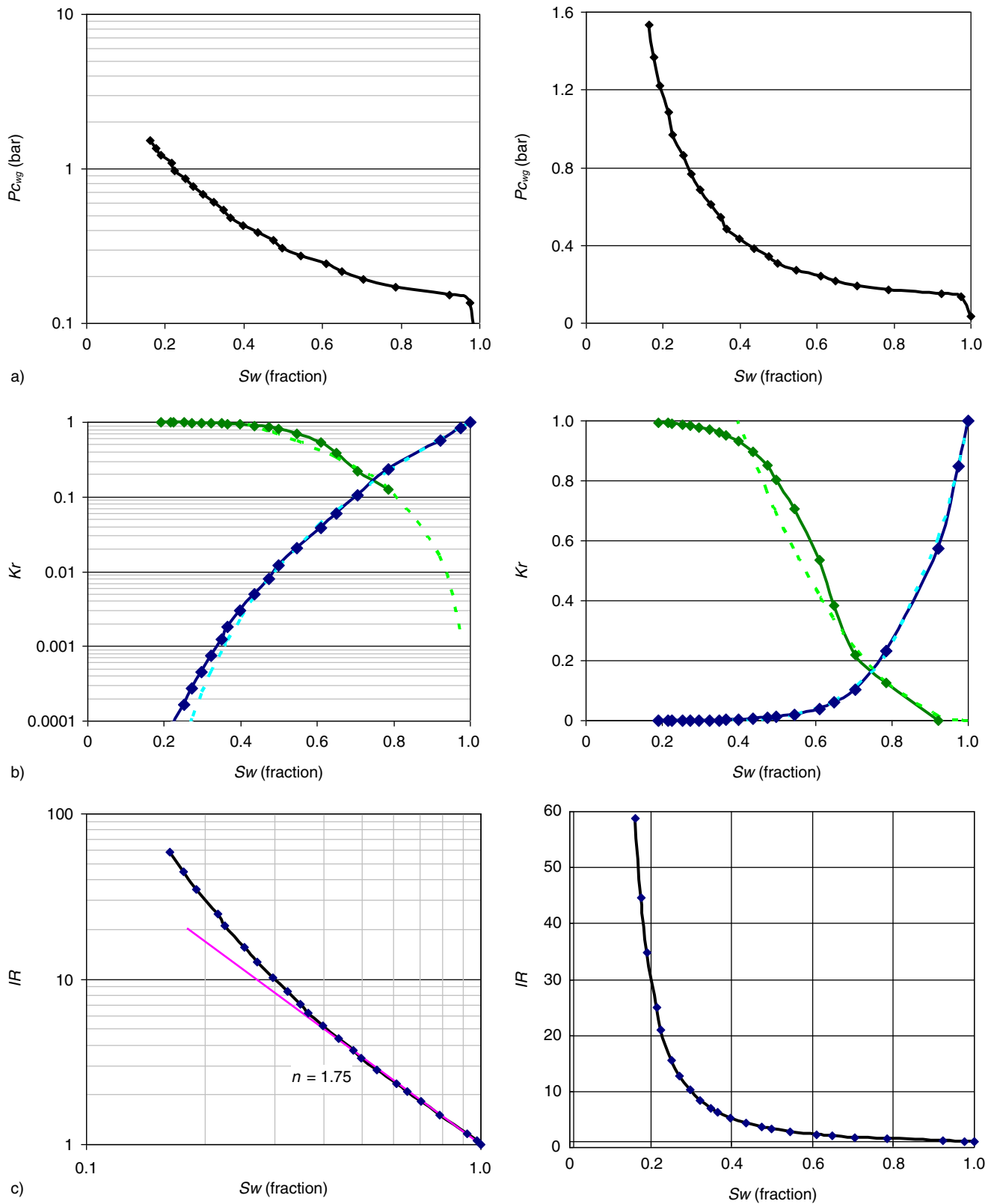


Figure 4

Simulation of the two phase flow properties during a drainage invasion of gas in logarithmic and linear coordinates: a) capillary pressure simulated with interfacial tension equal 78 dyne/cm; b) calculated relative permeability and corresponding Corey correlations with an exponent equal to 2 and 5.5 for gas and water, respectively (dotted lines); c) resistivity index $n = 1.75$.

The results are analysed in terms of the dimensionless numbers and the three dissolution regimes highlighted in the literature (Békri *et al.*, 1995).

2.3.1 Porosity and Permeability Evolution

The pore network built using Run #1 scenario is subjected to dissolution under various conditions, reflected by Pe and $PeDa$ dimensionless numbers. Evolution of porosity and permeability are shown in Figure 5. Three families of K - ϕ laws can be found depending on the localization of the mass transfer in the pore network:

- uniform dissolution which occurs when reaction is slow compared to diffusion. This case is characterized by a low value of $PeDa$, whatever the value of Pe , Figures 5a and 5b. In such a reaction limiting regime, the chemical disequilibrium ($c - c^*$) is uniform over the whole pore network;
- dissolution limited to the greatest pore-bodies (compact dissolution) which occurs when diffusion is the limiting factor. This regime is characterized by a slightly high to high value of $PeDa$ and a low value of Pe , Figures 5c-e. This means that diffusion is slow compared to reaction, but remains fast compared to flow. In such a case, disequilibrium remains in the largest elements (*i.e.*, pores bodies). Compared to uniform dissolution, permeability variations are very small: the contribution of pore-bodies to permeability is negligible when compared to the pore-throats contribution;
- reaction occurring along the main flow paths when the flow rate of the fluid and the reaction kinetic are high enough, *i.e.*, for high Pe and high $PeDa$ (Fig. 5d). In this regime, the chemical disequilibrium is no longer restricted to large elements. It is transported out of pore-bodies through the flow paths. Thus, dissolution occurs preferentially along flow paths and induces permeability variations larger than those associated to compact dissolution (Fig. 5).

The K - ϕ relationships which are derived from the PNM simulation (Fig. 5) can be implemented in the reservoir simulator as power regression. The exponent coefficients of the fitting function can be given as input tables depending on Pe and $PeDa$ (Tab. 3).

2.3.2 Macroscopic Reactive Transport Coefficients

The apparent reaction rate, the effective solute velocity and the dispersion coefficient are computed as functions of Pe and $PeDa$ before any modification of the pore network. These macroscopic coefficients are presented in Figure 6. $\bar{\gamma}^{/*}$ is the apparent reaction rate normalized by the reaction rate in perfect mixing conditions, $\bar{v}^{/*}$ is the normalization of the effective solute velocity by the mean interstitial

velocity of the fluid, whereas $\bar{D}^{/*}$ is the longitudinal dispersion normalized by the restricted diffusion coefficient of passive tracers.

At low $PeDa$, the reaction is so slow that the solute has time to spread by diffusion over the whole porous medium. As a consequence, a uniform reaction is induced. Under this condition, the structure of the rock does not play any role on the transport of the solute. Hence, $\bar{\gamma}^{*}$ is equal to the reaction rate in perfect mixing, the effective solute velocity \bar{v}^{*} is equal to the fluid velocity and the dispersion coefficient is equivalent to the dispersion coefficient of the passive tracer. This is in agreement with the results presented in Figure 6. The dispersion coefficient, at low $PeDa$ is also displayed in Figure 7 as a function of Pe . This representation of the longitudinal dispersion includes the mechanical dispersion, the boundary layer diffusion and the hold-up dispersion (Sahimi, 1995).

For high values of $PeDa$, the influence of the structure of the rock on the macroscopic coefficients is an increasing function of $PeDa$. Figure 6 shows a decrease of the apparent reaction rate, the velocity and the dispersion coefficients by increasing $PeDa$. When mass transfer is the limiting phenomenon (high values of $PeDa$), the reactions are mainly confined on the largest pore-bodies. Hence, only limited areas of the porous media are affected by the reaction. Thus on core scale, the apparent reaction is much slower than in case of perfect-mixing, the mean solute velocity is close to zero and the macroscopic dispersion coefficient depends only on the molecular diffusion (Fig. 6). Solute appears thus to be immobile.

CONCLUSION

A multi-scale PNM tool that takes into account pore and core scales is used to estimate the two phase flow properties and the reactive transport properties for single-phase flow as well as their dependency on dimensionless numbers. The approach is based on a local description of the physical phenomena that provides adequate macroscopic properties. The pore scale heterogeneities are taken into account by a conceptual representation of pore volume based on the routine petrophysical experimental data, namely the porosity, the permeability, the formation factor and the MICP.

Taking into account the geometry changes induced by the mineral reaction, the three phenomenological coefficients of transport and the porosity/permeability relationship on core scale are calculated as function of Pe and $PeDa$ for a sandstone sample taken from reservoir formation of the Pakoslaw gas field (near Załęcze-Żuchłów field, Poland).

It has been observed that the mean reactive solute velocity and dispersion can vary up to several orders of magnitude compared with the tracer values because of the variations of the pore scale solute concentration profile resulting from

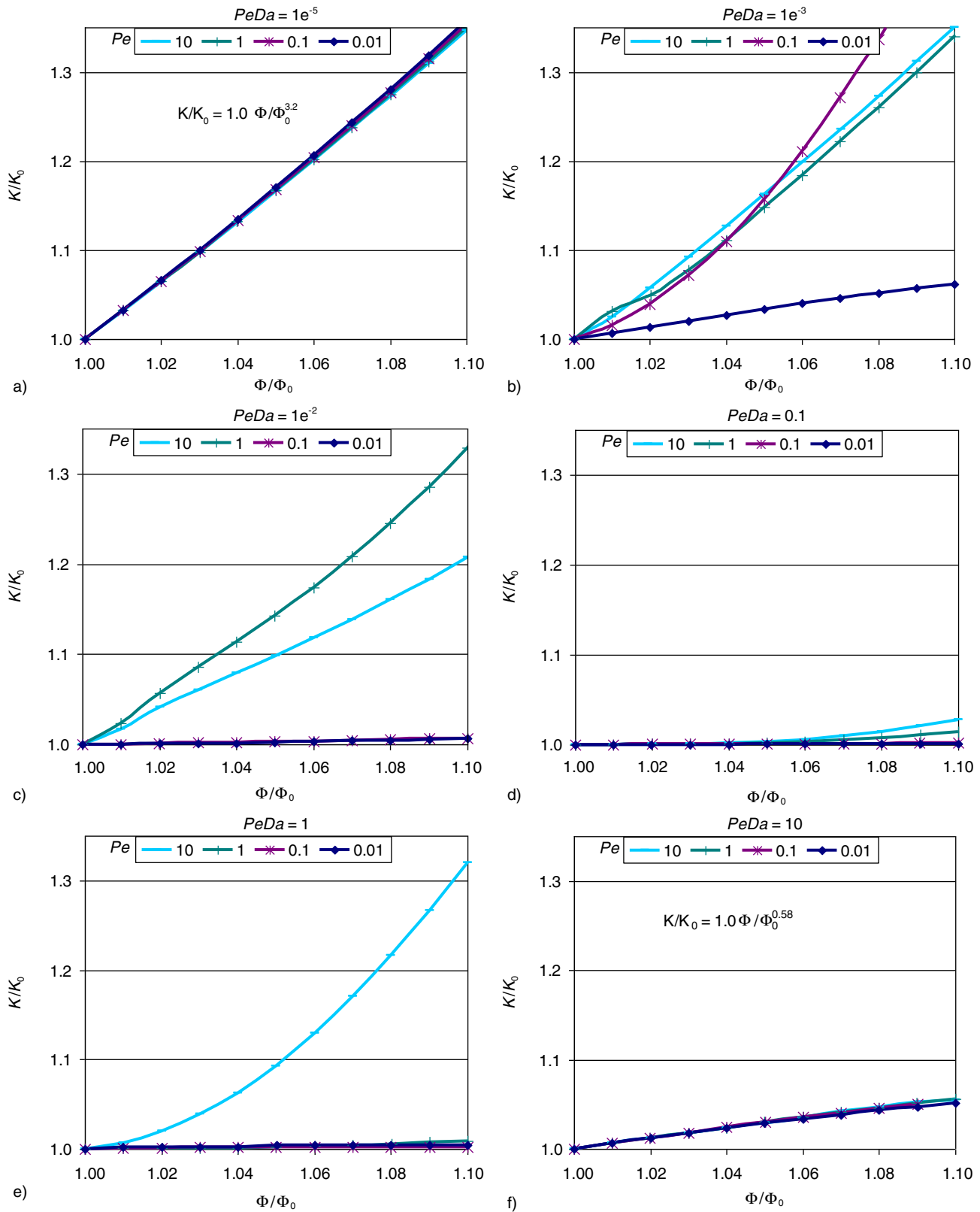


Figure 5

Porosity-permeability evolution for various values of Pe and $PeDa$. Sub-figures are for a fixed value of $PeDa$ number. They correspond to the columns of Table 3.

TABLE 3
Exponent coefficients of the fitting power regression function of the $K-\phi$ relationships depending on Pe and $PeDa$

$Pe \backslash PeDa$	0.00001	0.001	0.01	0.1	1	10
10	3.1	3.1	2	0.04-0.82	1.0-3.2	0.58
1	3.1	3.1	2.8	0.04-0.46	0.2	0.58
0.1	3.1	2.0-5.1	0.08	0.04	0.2	0.58
0.01	3.1	0.53	0.08	0.04	0.2	0.58

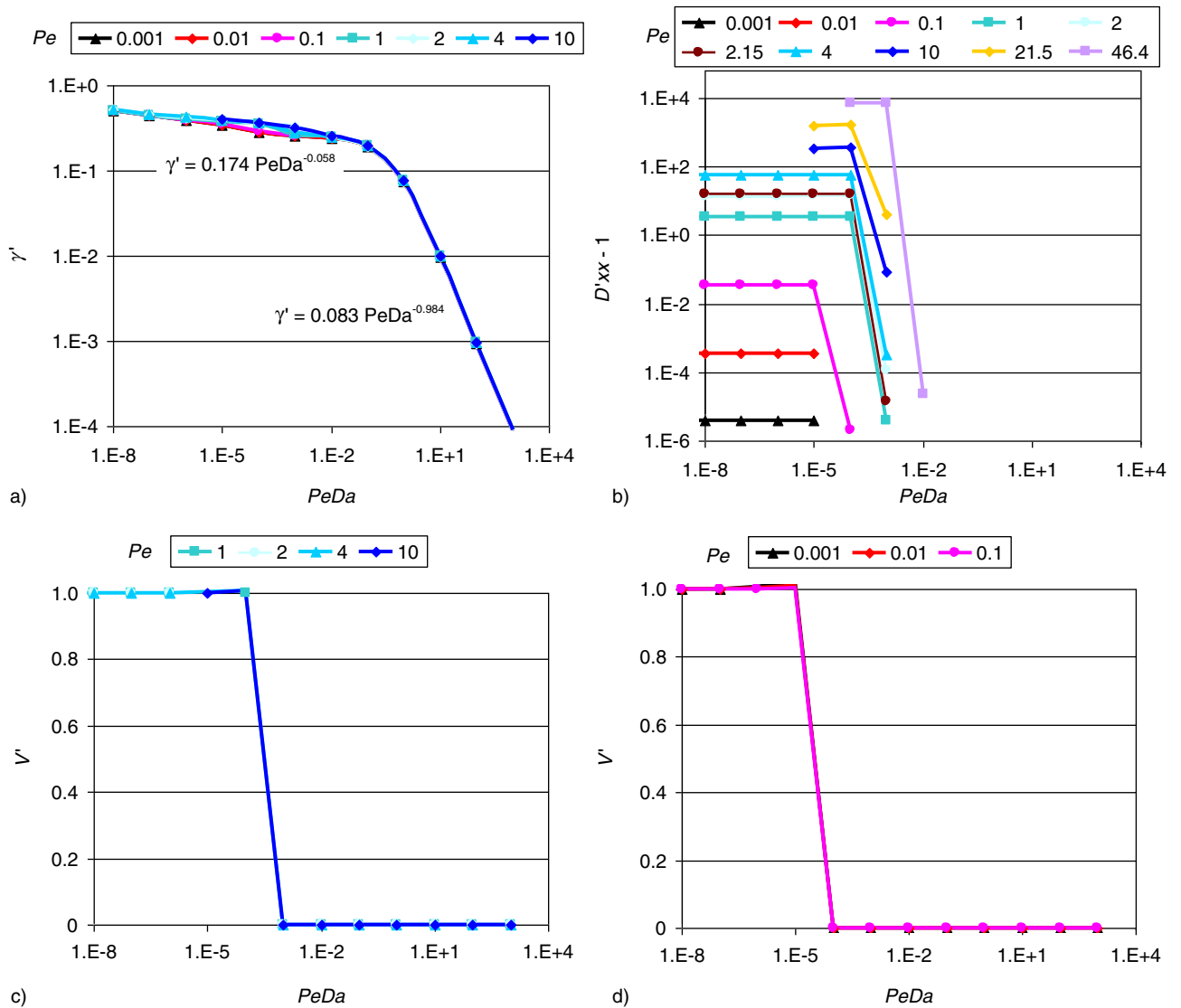


Figure 6

Macroscopic reactive transport coefficients on core scale as function of Pe and $PeDa$ before any geometry modification; a) dimensionless reactive macroscopic coefficients $\bar{\gamma}^*$; b) dimensionless dispersion macroscopic coefficients \bar{D}^* ; c) and d) dimensionless velocity macroscopic coefficients \bar{v}^* .

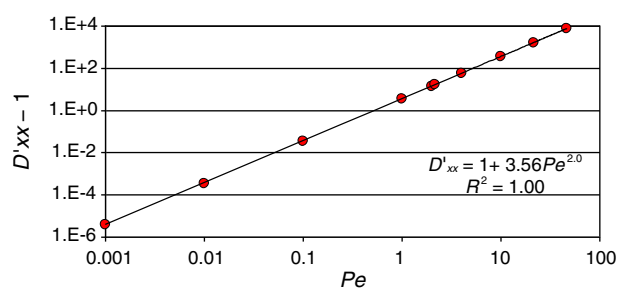


Figure 7

Dimensionless dispersion macroscopic coefficients ($\bar{D}^*_{xx} - 1$) as function of Pe for low $PeDa$ (i.e., for uniform dissolution).

mineral reactions. Similarly, when kinetics is limited by mass transfer, the reactive apparent coefficient can decrease by several orders of magnitude compared to the case of perfect-mixing.

The PNM results can be used as part of an integrated approach that takes into account pore, core and reservoir scales. These numerical results would have first to be validated by some dissolution and precipitation laboratory experiments. The properties determined by PNM simulation could then be used straightforwardly as input data for field scale simulation. Indeed, the output of the PNM simulation can be gathered in tables of dimensionless macroscopic coefficients as functions of Pe and $PeDa$ for a representative elementary volume of rock-type involved in the geological model. The grid-block properties at reservoir scale can be filled through the sub-grid properties determined by the PNM simulations. Of course, a sub-grid with different petrophysical properties and grid-block of different rock-types can be handled.

The approach is also used to determine the two phase flow properties of the considered rock, gas/water capillary pressure, relative permeabilities and resistivity index.

ACKNOWLEDGMENTS

This work is part of the SiteChar project: <http://www.sitechar-co2.eu>, Work Package 5. The research leading to these results has received funding from the European Union Seventh Framework Program (FP7/2007-2013) under grant agreement No. 256705.

REFERENCES

Adler P.M. (1992) *Porous media: geometry and transport*, Butterworth-Heinemann, Boston, USA.

Algive L., Békri S., Robin M., Vizika O. (2007) Reactive Transport: Experiments and Pore Network Modelling, Paper SCA2007-10 prepared for presentation at the *International Symposium of the Society of Core Analysts*, Calgary, Canada, 10-12 Sept., pp. 1-13.

Algive L., Békri S., Vizika O. (2010) Pore-network modeling dedicated to the determination of the petrophysical-property changes in the presence of reactive fluid, *SPE J.* **15**, 618-633.

Békri S., Laroche C., Vizika O. (2002) *Pore-network models to calculate transport properties in homogeneous and heterogeneous porous media*, Computational Methods in, Water Resources, pp. 1-8.

Békri S., Vizika O. (2006) Pore-network modeling of rock transport properties: application to a carbonate, Paper SCA2006-22 prepared for presentation at the *International Symposium of the Society of Core Analysts*, 12-16 Sept., Trondheim, Norway, pp. 1-12.

Békri S., Thovert J.F., Adler P.M. (1995) Dissolution of porous media, *Chem. Eng. Sci.* **50**, 2765-2791.

Blunt M., Zhou D., Fenwick D. (1995) Three-phase flow and gravity drainage in porous media, *Transp. Porous Med.* **20**, 77-103.

Corey A. (1954) The interrelation between gas and oil relative permeabilities, *Prod. Mon.* **19**, 38-41.

Dias M.M., Payatakes A.C. (1986) Network models for two-phase flow in porous media. Part 2. Motion of oil ganglia, *J. Fluid Mech.* **164**, 337-358.

van Dijke M., Sorbie K. (2002) Pore-scale network model for three-phase flow in mixed-wet porous media, *Phys. Rev. E.* **66**, 1-14.

Fatt I. (1956) The network model of porous media, *Trans. AIME* **207**, 144-181.

Fenwick D.H., Blunt M.J. (1998) Three-dimensional modeling of three-phase imbibition and drainage, *Adv. Water Resources* **21**, 2, 121-143.

Heiba A.A., Sahimi M., Scriven L.E., Davis H.T. (1992) Percolation theory of to-phase relative permeability, *SPE Reservoir Engineering* **7**, 123-132.

Hoefner M.L., Fohler H.S. (1988) Pore Evolution and Channel Formation During Flow and Reaction in Porous Media, *AIChE* **34**, 1, 45-54.

Izgec O., Demiral B., Bertin H., Akin S. (2008a) CO₂ Injection into Saline Carbonate Aquifer Formations II: Comparison of Numerical Simulations to Experiments, *Transp. Porous Med.* **73**, 57-74.

Izgec O., Demiral B., Bertin H., Akin S. (2008b) CO₂ injection into saline carbonate aquifer formations I: laboratory investigation, *Transp. Porous Med.* **72**, 1-24.

Kim D., Lindquist W.B. (2011) Dependence of pore-to-core up-scaled reaction rate on flow rate in porous media, *Transp. Porous Med.* **89**, 459-473.

Kim D., Peters C.A., Lindquist W.B. (2011) Upscaling geochemical reaction rates accompanying acidic CO₂-saturated brine flow in sandstone aquifers, *Water Resour. Res.* **47**, 1-49.

Laroche C., Vizika O., Kalaydjian F. (1999) Network modeling as a tool to predict three-phase gas injection in heterogeneous wettability porous media, *J. Petrol. Sci. Eng.* **24**, 155-168.

Laroche C., Vizika O. (2005) Two-phase flow properties prediction from small-scale data using pore-network modeling, *Transp. Porous Med.* **61**, 77-91.

Lemaitre R., Adler P.M. (1990) Fractal porous media IV: three-dimensional stokes flow through random media and regular fractals, *Transp. Porous Med.* **5**, 325-340.

- Li L., Peters C.A., Celia M. (2006) Upscaling geochemical reaction using pore-scale network modeling, *Adv. Water Resour.* **29**, 1351-1370.
- McDougall S.R., Sorbie K.S. (1997) Application of network modelling techniques to multiphase flow in porous media, *Petroleum Geoscience* **3**, 161-169.
- Mohanty K.K., Salter S.J. (1982) Multiphase flow in porous media: II. Pore-level modeling, *SPE paper* 11018, presented at the *57th Annual Technical Conference and Exhibition of the SPE AIME*, 26-29 Sept, New-Orleans, LA.
- Øren P. (2003) Reconstruction of Berea sandstone and pore-scale modelling of wettability effects, *J. Petrol. Sci. Eng.* **39**, 177-199.
- Øren P.E., Bakke S. (2002) Process based reconstruction of sandstones and prediction of transport properties, *Transp. Porous Med.* **46**, 311-343.
- Payatakes A.C., Dias M.M. (1984) Immiscible microdisplacement and ganglion dynamics in porous media, *Rev. Chem. Eng.* **2**, 85-174.
- Prat M. (1995) Isothermal drying of non-hygroscopic capillary porous materials as an invasion percolation process, *Int. J. Multiphase Flow* **21**, 5, 875-892.
- Press W.H., Flannery B.P., Teukolsky S.A., Vetterling W.T. (1992) *Numerical Recipes in C: The Art of Scientific Computing*, 2nd edn, Cambridge University Press, Cambridge, England.
- Sahimi M. (1995) *Flow and Transport in Porous Media and Fractured Rock*, VCH Verlagsgesellschaft mbH, Weinheim, Germany.
- Shapiro M., Brenner H. (1986) Taylor dispersion of chemically reactive species: irreversible first-order reactions in bulk and on boundaries, *Chem. Eng. Sci.* **41**, 1417-1433.
- Shapiro M., Brenner H. (1988) Dispersion of a chemically reactive solute in a spatially periodic model of a porous medium, *Chem. Eng. Sci.* **43**, 551-571.
- Sok R., Knackstedt M., Sheppard A., Pinczewski W., Lindquist W., Venkatarangan A., Paterson L. (2002) Direct and stochastic generation of network models from tomographic images; effect of topology on residual saturations, *Transp. Porous Med.* **46**, 345-371.
- Stewart T.L., Kim D.S. (2004) Modeling of biomass-plug development and propagation in porous media, *Biochem. Eng. J.* **17**, 107-119.
- Swoboda-Colberg N.G., Drever J.I. (1993) Mineral dissolution rates in plot-scale field and laboratory experiments, *Chem. Geol.* **105**, 51-69.
- Varloteaux C., Békri S., Adler P.M. (2013a) Pore network modelling to determine the transport properties in presence of a reactive fluid: From pore to reservoir scale, *Adv. Water Resour.* **53**, 87-100.
- Varloteaux C., Minh T.V., Békri S., Adler P.M. (2013b) Reactive transport in porous media: Pore-network model approach compared to pore-scale model, *Phys. Rev. E* **87**, 023010.
- Wood B., Radakovich K., Golfier F. (2007) Effective reaction at a fluid-solid interface: Applications to biotransformation in porous media, *Adv. Water Resour.* **30**, 1630-1647.
- Youssef S., Rosenberg E., Gland N., Békri S., Vizika O. (2007) Quantitative 3D characterisation of the pore space of real rocks: improved I-CT resolution and pore extraction methodology, Paper SCA2007-17 prepared for presentation at the *International Symposium of the Society of Core Analysts*, 10-12 Sept, Calgary, pp. 1-13.

Manuscript accepted in October 2014
Published online in January 2015